

Dalton Transactions

Accepted Manuscript



This article can be cited before page numbers have been issued, to do this please use: X. Wang, Y. He, Y. Ma, J. Liu, Y. Liu, Z. Qiao and Q. Huo, *Dalton Trans.*, 2018, DOI: 10.1039/C8DT02254B.



This is an Accepted Manuscript, which has been through the Royal Society of Chemistry peer review process and has been accepted for publication.

Accepted Manuscripts are published online shortly after acceptance, before technical editing, formatting and proof reading. Using this free service, authors can make their results available to the community, in citable form, before we publish the edited article. We will replace this Accepted Manuscript with the edited and formatted Advance Article as soon as it is available.

You can find more information about Accepted Manuscripts in the [author guidelines](#).

Please note that technical editing may introduce minor changes to the text and/or graphics, which may alter content. The journal's standard [Terms & Conditions](#) and the ethical guidelines, outlined in our [author and reviewer resource centre](#), still apply. In no event shall the Royal Society of Chemistry be held responsible for any errors or omissions in this Accepted Manuscript or any consequences arising from the use of any information it contains.



Journal Name

ARTICLE

Architecture yolk-shell structured mesoporous silica nanospheres for catalytic applications

Xue Wang,^{*a, b} Yapeng He,^c Yali Ma,^a Junmin Liu,^a Yunling Liu,^a Zhen-An Qiao^{*a} and Qisheng Huo^a

Received 00th January 20xx,
Accepted 00th January 20xx

DOI: 10.1039/x0xx00000x

www.rsc.org/

We report the design and realization of yolk-shell structured nanospheres with periodic mesoporous organosilica (PMO) nanospheres or noble metal nanoparticles encapsulated in mesoporous silica shells via a selected etching method. These architectures are well controlled in structure, size and morphology. The yolk-shell structured PMO@SiO₂ nanoparticles can be precisely functionalized with different catalytic functionalities even incompatible acidic and basic groups: PMO core with amino (-NH₂) groups and mesoporous silica shell with sulfonic acid (-SO₃H) groups. As a nanoreactor, the as-synthesized Au@SiO₂ nanospheres show faster reduction of 4-nitrophenol than nitrobenzene. Furthermore, the prepared PMO-NH₂@SiO₂-SO₃H nanoparticles can be used as bifunctional catalysts with highly efficient catalytic performance for catalyzing the deacetalization-Henry cascade reaction.

Introduction

Very recently, many scientific efforts have been directed toward the design and fabrication of mesoporous silica nanomaterials with controlled morphologies and tailored properties.¹⁻⁷ The yolk-shell nanostructures as an interesting family of complex new hollow nanoarchitectures have attracted tremendous attention, due to their outstanding structures in which a movable core is encapsulated inside a mesoporous shell and between the core and the outer shell of this material contains a void space.⁸⁻¹⁶ The void space of yolk-shell nanoparticles is expected to be useful for chemical storage, compartmentation, confinement of host-guest interactions and providing a unique environment for creating concerted actions between the core and a permeable shell.¹⁷⁻¹⁹ Furthermore, their unique physical and chemical properties such as low density, large surface area, high permeability, excellent loading capacity and functionality in both the cores and the outer shells, can

render yolk-shell nanoparticles attractive for applications in catalysis,^{18, 20, 21} drug delivery systems,²²⁻²⁴ and energy storage²⁵⁻²⁷ and surface-enhanced Raman scattering technologies.^{28, 29}

Up to now, several approaches have been developed for the synthesis of yolk-shell structured nanomaterials, such as selective etching approaches,³⁰⁻³² bottom-up or soft-templating,³³⁻³⁵ ship-in-bottle approach,³⁶ Ostwald ripening³⁷ or galvanic replacement process,³⁸ template-free approaches,³⁹ and Kirkendall effect based methods.^{40, 41} A wide range of chemical compositions of yolk-shell structured nanomaterials have been obtained, including metal NPs@silica,⁴² metal oxide@silica,⁴³ metal NPs@carbon,⁴⁴ metal NPs@metal oxide,⁴⁵ metal NPs@polymer,⁴⁶ silica@metal oxide,⁴⁷ silica@carbon,⁴⁸ polymer@polymer⁴⁹ and so on. However, the yolk-shell structured nanomaterials reported to date are generally composed of a catalytically active core, such as metal, metal oxide, and there are rare works that succeed in designing and utilizing catalytically active mesoporous shells, which limited their further applications as nanoreactors in cascade reactions. Therefore, the synthesis of yolk-shell structured nanomaterials with precisely located active sites both in the core and on the shell is still difficult and remains a great challenge.

In this work, with the aim of expanding the range of composition and functionality of the yolk-shell nanostructures, here we report on the construction of multifunctional yolk-shell structured nanomaterials consisting of a core of periodic mesoporous organosilica (PMO) spheres or Au nanoparticles, a hollow space

a State Key Laboratory of Inorganic Synthesis and Preparative Chemistry, College of Chemistry, Jilin University, Changchun 130012, China.

b Faculty of Chemistry and Chemical Engineering, Yunnan Normal University, Kunming 650500, China

c Faculty of Metallurgical and Energy Engineering, Kunming University of Science and Technology, Kunming 650093, China

E-mail: qjaozhenan@jlu.edu.cn; wangxue2468@126.com; Fax: +86-431-85168624; Tel: +86-431-85168602

† Electronic Supplementary Information (ESI) available: [details of TEM and images, DLS patterns, XRD curves, UV-vis absorbance and Table]. See DOI: 10.1039/x0xx00000x

between core and shell, and an outer silica shell with mesoporous channels. By using the versatile sol-gel chemistry, the catalytic functionalities including even incompatible acidic and basic groups could be located in yolk-shell structured nanoparticles with basic PMO core ($-NH_2$) and acidic silica shell ($-SO_3H$). These yolk-shell structured nanoparticles as nanoreactors show high catalytic efficiency for catalyzing the deacetalization-Henry cascade reaction. Besides, the as-synthesized $Au@SiO_2$ nanospheres were applied in 4-nitrophenol and nitrobenzene catalysis, respectively.

Experimental

Chemicals

TEOS was obtained from Sigma-Aldrich. Bis(trimethoxysilyl)ethane (BTEE) was obtained from Gelest. 3-Aminopropyltriethoxysilane (APTES), N-[3-(trimethoxysilyl) propyl] ethylenediamine (TSD), (3-mercaptopropyl) trimethoxysilane (MPTMS), benzaldehyde dimethyl acetal and benzaldehyde were purchased from Alfa Aesar. Toluene and malononitrile were obtained from Alading. Cetyltrimethylammonium bromide (CTAB) was obtained from Huishi Biochemical Reagent Company of China. $HAuCl_4 \cdot 3H_2O$ (99.7%) was purchased from Shanghai Chemical Corp. Ammonia solution (27 wt%), 4-nitrophenol, nitrobenzene, sodium borohydride ($NaBH_4$), hydrogen peroxide (H_2O_2 , 30 wt%), hydrofluoric acid (HF, 40 wt%), hydrochloric acid (HCl, 37 wt%), ethanol and methanol were purchased from Beijing Chemical Works. Deionized water was used in all experiments. All reagents were used without further purification.

Synthesis of yolk-shell structured $PMO@SiO_2$ and $Au@SiO_2$ nanoparticles

In a typical reaction, solution A (1.5 mL of TEOS in 13.5 mL of ethanol), solution B (20 mL of 27 wt% ammonia solution and 60 mL of ethanol) and solution C (100 μ L of TSD in 8 mL of ethanol) were prepared. 1.5 mL of periodic mesoporous organosilica (PMO) nanoparticles or 2 mL of Au nanoparticles dispersion solution was added into solution B and reacted for 10 min under vigorously stirring to form the cores. Then, solution C and identical volume of solution A were added into the reaction mixture synchronously at a rate of 1 mL/min, to form the middle layer of organosilica framework. Lastly, remaining solution A was added to form the outer layer of silica shell. The reaction was kept for 3 hours at 30 °C. The hybrid silica spheres were isolated by centrifugation and washed with ethanol and water repeatedly, and lastly resuspended in water. Yolk-shell structured $PMO@SiO_2$ or $Au@SiO_2$ nanoparticles were produced by etching the as-

prepared hybrid silica spheres with 10 wt% HF (aqueous solution). The product was sufficiently washed repeatedly with water. The preparation process of PMO and Au nanoparticles are shown in the Supplementary Information.

Synthesis of functional $PMO-NH_2@SiO_2-SO_3H$ nanoparticles

In the synthetic procedure of $PMO@SiO_2$ nanoparticles, using the same amount of $PMO-NH_2$ nanoparticles dispersion solution replaced PMO nanoparticles dispersion solution, remaining solution A and 60 μ L of MPTMS were added to form the outer layer of silica shell, functional $PMO-NH_2@SiO_2-SH$ nanoparticles were obtained. Then, 1 g of $PMO-NH_2@SiO_2-SH$ nanoparticles were dispersed in 40 g of H_2O_2 (30 wt%) and stirred at RT for 24 h before centrifugation. 1 g of dried sample was then stirred in 200 mL of HCl (0.01 M) for 12 h at RT for acidification. After being thoroughly washed with deionized water, the solid product was dried at 60 °C overnight. $PMO-NH_2@SiO_2-SO_3H$ nanoparticles were prepared.

Catalytic reduction of 4-nitrophenol and nitrobenzene using $Au@SiO_2$ nanoparticles as catalysts

Ten milligrams of $Au@SiO_2$ nanoparticles were homogeneously dispersed in 10 mL of deionized water by ultrasonication. 0.3 mL of 4-nitrophenol or nitrobenzene solution (1 mM) and 0.65 mL of $NaBH_4$ aqueous solution (0.2 M) were added to 2 mL of water. Then, 0.1 mL of $Au@SiO_2$ nanoparticles solution was added to the mixture. During the reaction, the mixture was taken at regular intervals and analyzed by UV-visible spectroscopy.

One-pot deacetalization-Henry cascade reaction

0.1 g of the solid catalyst, 0.076 g of benzaldehyde dimethyl acetal (0.5 mmol), 0.046 g of malononitrile (0.7 mmol) and 4 mL of toluene were added under nitrogen. The mixture was stirred at 90 °C under nitrogen atmosphere for 12 h.

Characterisation

TEM images were obtained on FEI Tecnai G² F20 s-twin D573 field emission transmission electron microscope with an accelerating voltage of 200 kV. SEM images were obtained on a JEOL JSM-6700F field-emission scanning electron microscope. The particle size was measured by photon correlation spectroscopy employing a Nano ZS90 laser particle analyzer (Malvern Instruments, UK) at 25 °C. Nitrogen adsorption-desorption isotherms were obtained at -196 °C on a Micromeritics ASAP 2420 surface area analyzer. Samples were degassed at 150 °C for a minimum of 12 h prior to analysis. Brunauer-Emmett-Teller (BET) surface areas were calculated from the linear part of the

BET plot. Pore size distribution was estimated from the adsorption branch of the isotherm by the BJH method. Powder XRD patterns were obtained by using a Rigaku 2550 diffractometer with Cu K α radiation ($\lambda=1.5418$ Å). The infrared spectra (IR) of samples were recorded in KBr disks using a Bruker IFS 66 V/S FTIR spectrometer. The X-ray photoelectron measurements were performed using a Thermo Escalab 250 spectrometer with monochromatized Al K α excitation. Gas chromatography-mass spectrometry (GC-MS) were performed using GCMS-QP 2010 Plus. The elemental analyses (C, H, N and S) were carried out with a Vario EL cube elemental analyzer.

Results and discussion

In this synthesis, our group have succeeded in fabricating a kind of yolk-shell structure: a special hollow nanosphere with mesoporous silica shell and periodic mesoporous organosilica (PMO) or Au inner core by selective etching of organic-inorganic hybrid silica spheres with a three-

layer sandwich structure, using N-[3-(trimethoxysilyl) propyl] ethylenediamine (TSD) condensed with tetraethylorthosilane as an etchable layer. Figure S1a, b show the scanning electron microscopy (SEM) and transmission electron microscopy (TEM) images of PMO nanoparticles with size about ~ 280 nm, prepared by a reported method in our group.⁵⁰ Figure S1c shows that PMO nanoparticles possessing highly ordered pore structure. The TEM and SEM images of hybrid silica spheres with PMO nanoparticles as the inner cores show that the nanoparticles have uniform spherical morphology in large domains and the particles diameter is ~ 600 nm (Figure 1a and b). After etching with aqueous hydrofluoric acid (HF), the hybrid silica spheres were converted into yolk-shell structure with mesoporous SiO₂ outer shell and PMO inner core, the shell thicknesses are roughly estimated at about ~ 25 nm (Figure 1c and d). The PMO@SiO₂ nanoparticles are reduced compared to those of the hybrid silica spheres, resulting from the shrinkage of silica during etching process. The present selective etching strategy can be also applied for fabricating yolk-

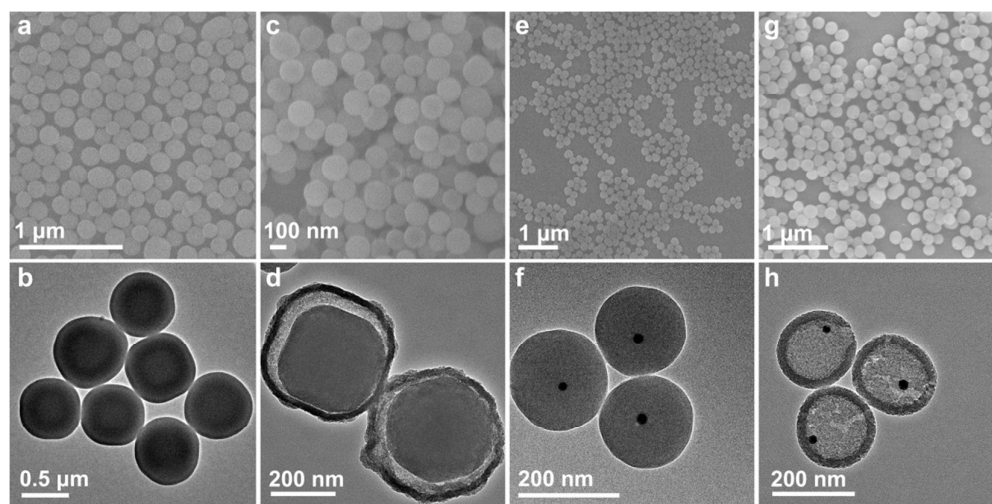
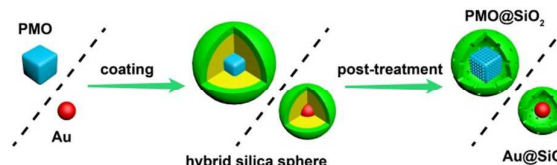


Figure 1. SEM and TEM images of (a), (b) hybrid silica spheres with PMO inner cores; (c), (d) yolk-shell structured PMO@SiO₂ nanospheres; (e), (f) hybrid silica spheres with Au inner cores; (g), (h) yolk-shell structured Au@SiO₂ nanospheres.

shell structured Au@SiO₂ nanoparticles. For example, by using Au nanoparticles (Figure S1d) replace PMO nanoparticles, hybrid Au/SiO₂ nanospheres were first synthesized (Figure 1e and f) and then successfully converted into yolk-shell structure under etching conditions in HF solution (Figure 1g and h). The successful encapsulation of Au nanoparticles within the mesoporous silica shell could also be evidenced by X-ray diffraction (XRD) characterization (Figure S2). Four diffraction peaks can be seen in the 2θ range 30-90°, assigned to (111), (200), (220), and (311) reflections of the cubic (fcc) Au nanoparticles lattice, respectively. It indicates the presence of crystalline Au nanoparticles at Au@SiO₂

nanoparticles. The whole synthesis process of the yolk-shell PMO@SiO₂ or Au@SiO₂ nanospheres is schematically represented in Scheme 1.



Scheme 1. Schematics of the synthetic procedures of yolk-shell structured PMO@SiO₂ and Au@SiO₂ nanospheres.

Journal Name

ARTICLE

Dynamic light scattering (DLS) measurements carried out in water (Figure 2a) show the hydrodynamic diameters of the PMO nanoparticles, hybrid silica nanospheres and PMO@SiO₂ samples. The DLS curves of two different nanospheres show that the hydrodynamic diameter of the hybrid silica nanospheres is larger than that of the PMO@SiO₂ nanoparticles, which are very close to those measured by TEM. More importantly, the polydispersity index of these samples is approximately 1%, thus indicating a high uniformity in the sizes of these samples. The DLS results of hybrid Au/SiO₂ nanospheres and Au@SiO₂ nanoparticles are shown in Figure S3. The small-angle X-ray diffraction (SAXRD) analysis of three different nanoparticles is shown in Figure 2b. The PMO nanoparticles not only exhibit three well-resolved peaks in the range of 1.5° < 2θ < 2.5° that can be indexed as the (200), (210), and (211) reflections but also three peaks assignable to the (320), (321), and (400) planes (2.5° < 2θ

< 4°), indicating a typical cubic (*Pm3n*) mesostructure. For the hybrid silica nanospheres, because of the PMO nanoparticles are coated by solid SiO₂ shell, there is no diffraction peak in SAXRD pattern. The PMO@SiO₂ samples show three diffraction peaks in the 2θ angle range of 1.5°-2.5°, but the peak intensity weakens, which confirms a markedly decreased long-range ordering compared to PMO samples with the formation of wormlike mesostructured shell. To further confirm the mesoporous structure of the three different samples, we use nitrogen adsorption/desorption analysis. The N₂ sorption isotherm (Figure 2c) of PMO nanoparticles and PMO@SiO₂ nanoparticles show a type IV isotherm and the pore size distribution (Figure 2d) centered at 3 nm, these results further suggest that the obtained samples possess mesopores. The hybrid silica spheres show only external surfaces.

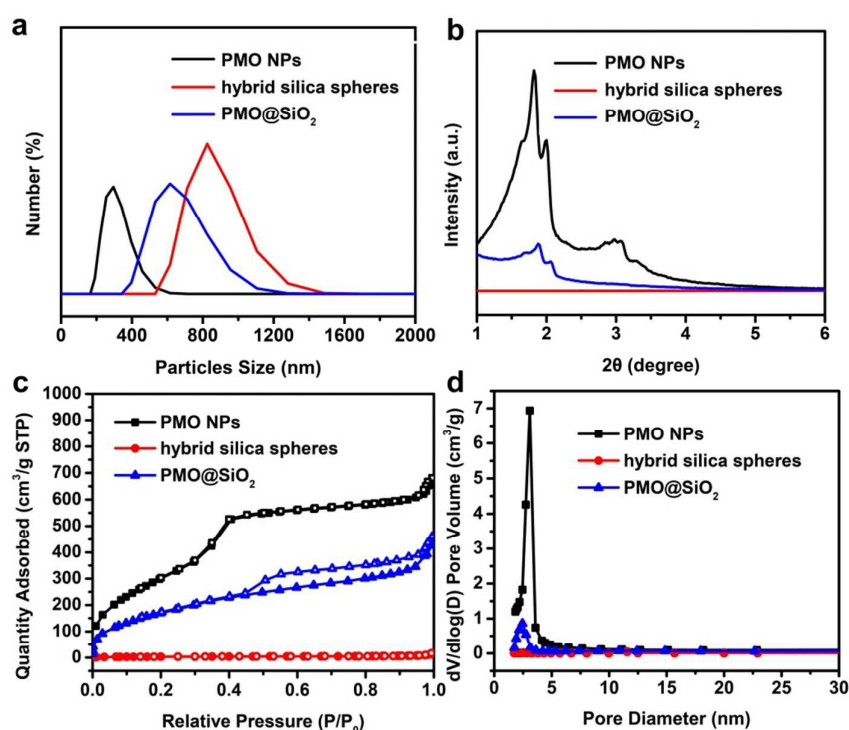


Figure 2. (a) Hydrodynamic diameters; (b) the small-angle XRD patterns; (c) nitrogen adsorption/desorption isotherms and (d) pore size distribution curves of PMO nanoparticles, hybrid silica spheres and yolk-shell structured PMO@SiO₂ nanoparticles.

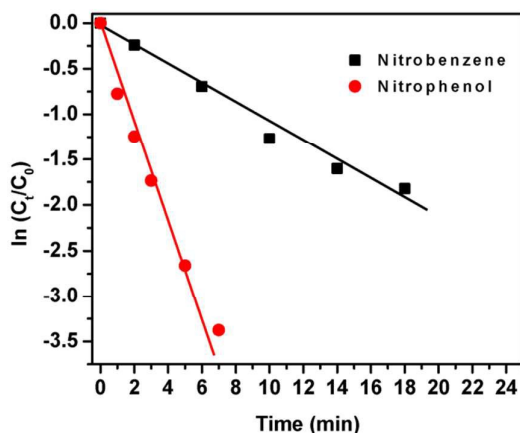


Figure 3. Kinetic analysis of the catalytic reactions and plot of $\ln(C_t/C_0)$ versus time for 4-nitrophenol and nitrobenzene.

The catalytic activity of yolk-shell structured Au@SiO_2 nanoparticles for the reduction of 4-nitrophenol (4-NP) to 4-aminophenol (4-AP) and nitrobenzene to aminobenzene are examined. The evolution of UV-visible spectra with the reaction time for the reduction of 4-NP to 4-AP and nitrobenzene to aminobenzene with Au@SiO_2 nanoparticles as catalysts are monitored (Figure S4). In the case of 4-NP, the peak at 400 nm, which is due to the 4-nitrophenolate ions, decreases with reaction time, and a new peak appears at 300 nm, which is a result of the production of 4-AP (Figure S4a). In the case of reduction of nitrobenzene, the characteristic absorption peak of nitrobenzene at 275 nm weakens with reaction time and the absorption peak of aminobenzene at 232 nm increases, which indicates the reduction of nitrobenzene to aminobenzene (Figure S4b). The kinetic analysis of the reactions can be carried out as described from the temporal decay of these peaks. The same amount of catalyst was used in each reaction. The ratio of C_t and C_0 , where C_t and C_0 are 4-nitrophenol or nitrobenzene concentrations at time t and 0, respectively, was measured from the relative intensity of the respective absorbances, A_t/A_0 . The linear relations of $\ln(C_t/C_0)$ versus time indicate that the reactions followed the first-order kinetics. The apparent rate constants were estimated from diffusion-coupled first order reaction kinetics using the slopes of straight lines in Figure 3. The apparent rate constant obtained for the reduction of 4-nitrophenol ($k_{\text{app}}=0.52 \text{ min}^{-1}$) was now one order higher than that of nitrobenzene ($k_{\text{app}}=0.11 \text{ min}^{-1}$), which suggests that the hydrophilic SiO_2 shell favors the diffusion of more hydrophilic 4-NP into the core region of the yolk-shell catalysts.⁵¹ Compared with other reported Au/SiO_2 based catalysts for the reduction of 4-nitrophenol, the prepared Au@SiO_2 nanoparticles show high catalytic activity, as summarized in Table S1.⁵²⁻⁶⁰

By a co-condensation method, the PMO nanoparticles could be functionalized with 3-aminopropyltriethoxysilane (APTES) and the mesoporous SiO_2 outer shell could be functionalized with (3-mercaptopropyl)trimethoxysilane (MPTMS), we successfully prepare novel $\text{PMO-NH}_2@SiO_2-SH$ nanoparticles, which make these yolk-shell structured nanoparticles owning multifunctional properties. $\text{PMO-NH}_2@SiO_2-SO_3H$ nanoparticles with basic PMO cores and acidic SiO_2 shells can be facily obtained through post-treatment of $\text{PMO-NH}_2@SiO_2-SH$ by oxidation of the SH to SO_3H groups using H_2O_2 .

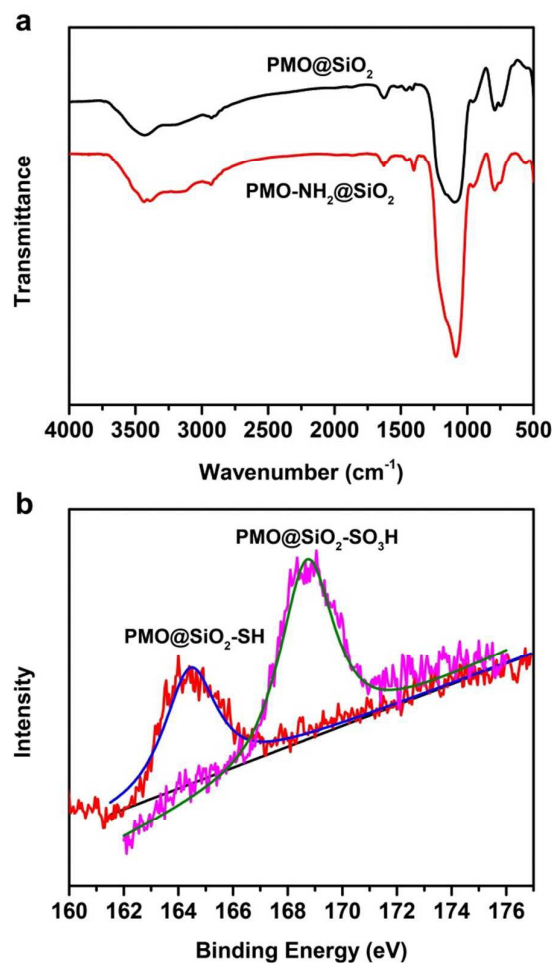


Figure 4. (a) IR spectra of PMO@SiO_2 and $\text{PMO-NH}_2@SiO_2$ nanoparticles; (b) S 2p XPS spectra of PMO@SiO_2-SH and PMO@SiO_2-SO_3H nanoparticles.

The incorporated NH_2 and SO_3H groups in $\text{PMO-NH}_2@SiO_2-SO_3H$ nanoparticles are verified by IR spectroscopy and X-ray photoelectron spectroscopy (XPS) (Figure 4). The IR spectrum of $\text{PMO-NH}_2@SiO_2-SO_3H$ nanoparticles display characteristic peaks at 2850-3000 cm^{-1} and 1600 cm^{-1} attributed to NH vibration of amine groups (Figure 4a). The existence of SH and SO_3H groups are confirmed by XPS analysis. For PMO@SiO_2-SH

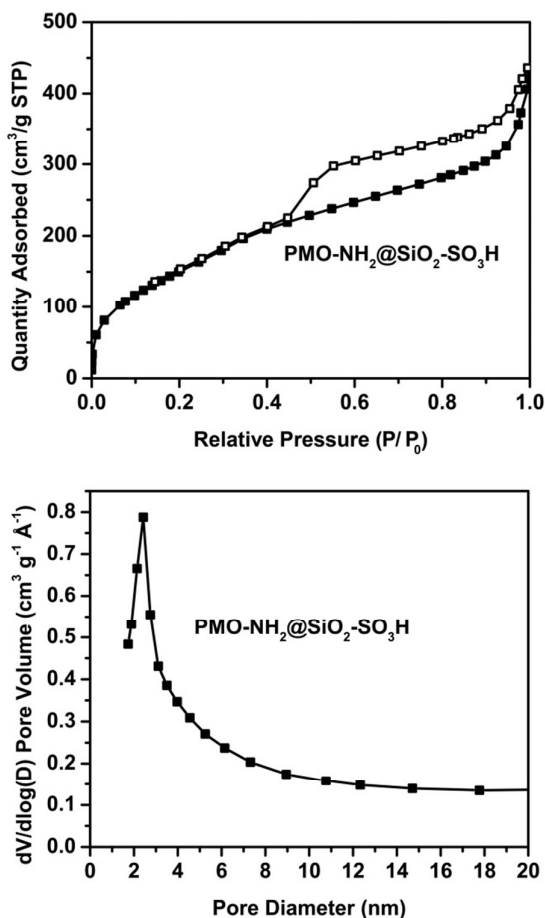
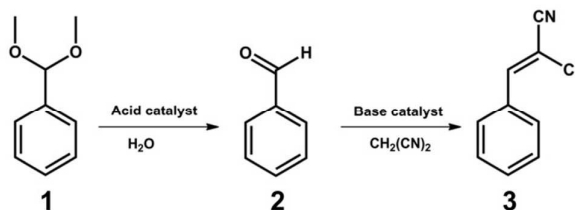


Figure 5. (a) Nitrogen adsorption/desorption isotherms and (b) pore size distribution curves of functional PMO-NH₂@SiO₂-SO₃H nanoparticles.

nanoparticles, a prominent peak indicative of S²⁻ (located at 164 eV) can be observed; for PMO@SiO₂-SO₃H sample, the XPS curve shows a prominent peak at 169 eV indicating for the presence of higher oxidized sulphur forms (Figure 4b). According to the XPS data, the SH groups can be oxidized to SO₃H groups in our experiment. The successful location of different types of functional groups in PMO-NH₂@SiO₂-SH nanoparticles is attributed to the separate steps for preparation of PMO nanoparticles and yolk-shell nanoparticles. Thus, it is possible to precisely locate the active sites in the PMO nanoparticles or on the SiO₂ shell of PMO-NH₂@SiO₂-SO₃H nanoparticles through controlled addition of functional groups at different synthetic steps. The N and S contents of the PMO-NH₂@SiO₂-SO₃H samples are 2.17% and 2.95%, respectively, based on the results of CHNS elemental analysis. Since most of the N element comes from NH₂ groups and the S element comes from SO₃H groups, the content of NH₂ and SO₃H is 2.48% and 7.47% in PMO-NH₂@SiO₂-SO₃H samples, respectively.

The SEM and TEM images of PMO-NH₂@SiO₂-SO₃H nanoparticles show that the morphology and pore structure of bifunctionalized PMO-NH₂@SiO₂-SO₃H nanoparticles are the same as for the unfunctionalized PMO@SiO₂ nanoparticles (Figure S5). The DLS result shows that the hydrodynamic diameter of PMO-NH₂@SiO₂-SO₃H and PMO@SiO₂ nanoparticles have nearly the same size (Figure S6). The small-angle XRD pattern and N₂ sorption isotherms of functional PMO-NH₂@SiO₂-SO₃H nanoparticles further indicate the existence of mesoporous structures. For the small-angle XRD pattern of PMO-NH₂@SiO₂-SO₃H nanoparticles, the peak intensity weakens as the NH₂ and SO₃H groups adds (Figure S7), implying that the NH₂ and SO₃H groups would perturb the self-assembly of surfactant micelles and the silica precursors. Figure 5a shows the N₂ sorption isotherms of PMO-NH₂@SiO₂-SO₃H nanoparticles. Compared with PMO@SiO₂ nanoparticles, the adsorbed amount of PMO-NH₂@SiO₂-SO₃H nanoparticles decrease, this is because of the functionalized groups in the framework occupy part of the pore. The pore size distribution patterns of PMO-NH₂@SiO₂-SO₃H nanoparticles shows that the pore diameter is about 2.2 nm (Figure 5b).

Table 1. Schematic illustration of the multistep reaction sequence involving acidic catalysis and basic catalysis for the synthesis of benzylidenemalononitrile and acid-base reaction sequences by different catalysts.



Catalysts	Coverion of 1 (%)	Yield of 2 (%)	Yield of 3 (%)
PMO-NH ₂ @SiO ₂ -SO ₃ H	>99	Trace	>99
PMO-NH ₂ @SiO ₂	Trace	Trace	Trace
PMO@SiO ₂ -SO ₃ H	>99	>99	Trace
Physical mixture of PMO-NH ₂ @SiO ₂ and PMO@SiO ₂ -SO ₃ H	35	Trace	35

Owing to its structural features, the yolk-shell structured PMO-NH₂@SiO₂-SO₃H nanoparticles can be used as a nanoreactor for the acid-basic cascade reaction. The catalytic performance of PMO-NH₂@SiO₂-SO₃H,

PMO@SiO₂-SO₃H, PMO-NH₂@SiO₂ and PMO@SiO₂ nanoparticles on the acid-basic cascade reaction of benzaldehyde dimethylacetal to benzylidenemalononitrile is shown in Table 1. PMO-NH₂@SiO₂-SO₃H nanoparticles show superior catalytic activity for the acid-basic cascade reaction. 100% conversion of benzaldehyde dimethylacetal and >99% yield of benzylidenemalononitrile are realized after the reaction. However, the PMO@SiO₂-SO₃H nanoparticles only show the highest catalytic activity in the catalytic reaction of benzaldehyde dimethylacetal to benzaldehyde, and PMO-NH₂@SiO₂ or PMO@SiO₂ nanoparticles cannot catalyze the acid-basic cascade reaction. This finding suggests that acidic SO₃H groups on the SiO₂ shells and basic NH₂ groups on the PMO yolks are efficiently separated by the unique structure, without occurs of neutralization. The integration of both the acidic and basic functional groups in the yolk-shell nanoreactor can shorten the reaction pathway. Furthermore, the high yield and selectivity of the PMO-NH₂@SiO₂-SO₃H nanoparticles suggest that the appropriate location of the active sites in the yolk-shell structure is essential to make different kinds of functional groups work efficiently during the catalytic process, especially for the groups that are incompatible with each other.

Conclusions

In summary, yolk-shell structured nanoparticles with two kinds of different compositions: PMO nanospheres and Au nanoparticles as the cores encapsulated in mesoporous silica shells were prepared. By a co-condensation method, the PMO@SiO₂ nanoparticles could be functionalized with different catalytic groups (even incompatible acidic and basic groups) in a controllable manner: PMO cores with NH₂ groups and mesoporous silica shell with SO₃H groups. More importantly, as the bifunctional catalysts for catalyzing the deacetalization-Henry cascade reaction, the prepared PMO-NH₂@SiO₂-SO₃H nanoparticles show highly efficient catalytic performance. Besides, the as-synthesized yolk-shell Au@SiO₂ nanospheres were applied in 4-nitrophenol and nitrobenzene catalysis, respectively.

Acknowledgements

This work was supported by the Young Thousand Talented Program, the National Natural Science Foundation of China (Grant No. 2162200022, 21671073, 21671074, 21621001, 21371067 and 21373095) and the Doctoral Fund of Yunnan Normal University (No. 2017ZB015).

Notes and references

1. M. Wu, Y. Chen, L. Zhang, X. Li, X. Cai, Y. Du, L. Zhang and J. Shi, *J. Mater. Chem. B*, 2015, **3**, 766-775.
2. K. Moeller, J. Kobler and T. Bein, *Adv. Funct. Mater.*, 2007, **17**, 605-612.
3. X. Wang, Y. Zhang, W. Luo, A. A. Elzatahry, X. Cheng, A. Alghamdi, A. M. Abdullah, Y. Deng and D. Zhao, *Chem. Mater.*, 2016, **28**, 2356-2362.
4. W. Wang, P. Wang, X. Tang, A. A. Elzatahry, S. Wang, D. Al-Dahyan, M. Zhao, C. Yao, C. T. Hung, X. Zhu, T. Zhao, X. Li, F. Zhang and D. Zhao, *ACS central science*, 2017, **3**, 839-846.
5. W. Wang, H. Long, T. Li, Y. Wang, S. Liu and H. Ru, *Micro. Meso. Mater.*, 2018, **258**, 262-268.
6. R. Liu, Y. Zhang, X. Zhao, A. Agarwal, L. J. Mueller and P. Feng, *J. Am. Chem. Soc.*, 2010, **132**, 1500-1501.
7. R. Liu, P. Liao, J. Liu and P. Feng, *Langmuir*, 2011, **27**, 3095-3099.
8. J. Liu, S. Z. Qiao, S. B. Hartono and G. Q. Lu, *Angew. Chem., Inter. Ed.*, 2010, **49**, 4981-4985.
9. L. S. Lin, X. Yang, Z. Zhou, Z. Yang, O. Jacobson, Y. Liu, A. Yang, G. Niu, J. Song, H. H. Yang and X. Chen, *Adv. Mater.*, 2017, **29**.
10. J. Wang, W. Li, F. Wang, Y. Xia, A. M. Asiri and D. Zhao, *Nanoscale*, 2014, **6**, 3217-3222.
11. M. Qiao, X. Lei, Y. Ma, L. Tian, X. He, K. Su and Q. Zhang, *Nano Res.*, 2018, **11**, 1500-1519.
12. J. Liu, S. Z. Qiao, J. S. Chen, X. W. Lou, X. Xing and G. Q. Lu, *Chem. Commun.*, 2011, **47**, 12578-12591.
13. B. Jin, E. Jung, M. Ma, S. Kim, K. Zhang, J. I. Kim, Y. Son and J. H. Park, *J. Mater. Chem. A*, 2018, **6**, 2585-2592.
14. X. W. Lou, L. A. Archer and Z. Yang, *Adv. Mater.*, 2008, **20**, 3987-4019.
15. L. L. Xing, G. G. Zhao, K. J. Huang and X. Wu, *Dalton T.*, 2018, **47**, 2256-2265.
16. L. S. Lin, J. Song, H. H. Yang and X. Chen, *Adv. Mater.*, 2018, **30**.
17. Y. Yang, X. Liu, X. Li, J. Zhao, S. Bai, J. Liu and Q. Yang, *Angew. Chem., Inter. Ed.*, 2012, **51**, 9164-9168.
18. Y. Chen, Q. Wang and T. Wang, *Dalton T.*, 2015, **44**, 8867-8875.
19. R. Purbia and S. Paria, *Nanoscale*, 2015, **7**, 19789-19873.
20. J. Liu, H. Q. Yang, F. Kleitz, Z. G. Chen, T. Yang, E. Strounina, G. Q. Lu and S. Z. Qiao, *Adv. Funct. Mater.*, 2012, **22**, 591-599.
21. Q. Yue, J. Li, Y. Zhang, X. Cheng, X. Chen, P. Pan, J. Su, A. A. Elzatahry, A. Alghamdi, Y. Deng and D. Zhao, *J. Am. Chem. Soc.*, 2017, **139**, 15486-15493.
22. Y. Chen, H. Chen, M. Ma, F. Chen, L. Guo, L. Zhang and J. Shi, *J. Mater. Chem.*, 2011, **21**, 5290-5298.
23. C. Zhang, Z.-C. Yao, Q. Ding, J. J. Choi, Z. Ahmad, M.-W. Chang and J.-S. Li, *Acs Appl. Mater. Inter.*, 2017, **9**, 21485-21495.
24. L. Zhang, S. Qiao, Y. Jin, Z. Chen, H. Gu and G. Q. Lu, *Adv. Mater.*, 2008, **20**, 805-809.
25. J. Zhang, K. Wang, Q. Xu, Y. Zhou, F. Cheng and S. Guo, *Acs Nano*, 2015, **9**, 3369-3376.
26. H. Hu, B. Guan, B. Xia and X. W. Lou, *J. Am. Chem. Soc.*, 2015, **137**, 5590-5595.

ARTICLE

Journal Name

27. W. M. Zhang, J. S. Hu, Y. G. Guo, S. F. Zheng, L. S. Zhong, W. G. Song and L. J. Wan, *Adv. Mater.*, 2008, **20**, 1160-1165.
28. M. Roca and A. J. Haes, *J. Am. Chem. Soc.*, 2008, **130**, 14273-14279.
29. G. Chen, Y. Wang, M. Yang, J. Xu, S. J. Goh, M. Pan and H. Chen, *J. Am. Chem. Soc.*, 2010, **132**, 3644-3645.
30. L. Li, D. Qin, X. Yang and G. Liu, *Polymer Chemistry*, 2010, **1**, 289-295.
31. G. L. Li and X. L. Yang, *J. Phys. Chem. B*, 2007, **111**, 12781-12786.
32. Q. Zhang, J. Ge, J. Goebel, Y. Hu, Z. Lu and Y. Yin, *Nano Research*, 2009, **2**, 583-591.
33. Y. S. Li and J. L. Shi, *Adv. Mater.*, 2014, **26**, 3176-3205.
34. R. Liu, Y. W. Yeh, V. H. Tam, F. Qu, N. Yao and R. D. Priestley, *Chem. Commun.*, 2014, **50**, 9056-9059.
35. J. Liu, R. Harrison, J. Z. Zhou, T. T. Liu, C. Yu, G. Q. Lu, S. Z. Qiao and Z. P. Xu, *J. Mater. Chem.*, 2011, **21**, 10641-10644.
36. X. W. Lou, C. L. Yuan, E. Rhoades, Q. Zhang and L. A. Archer, *Adv. Funct. Mater.*, 2006, **16**, 1679-1684.
37. L. Bin and Z. H. Chun, *Small*, 2005, **1**, 566-571.
38. E. C. Cho, P. H. Camargo and Y. Xia, *Adv. Mater.*, 2010, **22**, 744-748.
39. C. Galeano, C. Baldizzone, H. Bongard, B. Spliethoff, C. Weidenthaler, J. C. Meier, K. J. J. Mayrhofer and F. Schüth, *Adv. Funct. Mater.*, 2014, **24**, 220-232.
40. X. Huang, M. G. Willinger, H. Fan, Z. L. Xie, L. Wang, A. Klein-Hoffmann, F. Girgsdies, C. S. Lee and X. M. Meng, *Nanoscale*, 2014, **6**, 8787-8795.
41. Y. D. Yin, R. M. Rioux, C. K. Erdonmez, S. Hughes, G. A. Somorjai and A. P. Alivisatos, *Science*, 2004, **304**, 711-714.
42. J. Lee, J. C. Park and H. Song, *Adv. Mater.*, 2008, **20**, 1523-1529.
43. G. Li, E. T. Kang, K. G. Neoh and X. Yang, *Langmuir*, 2009, **25**, 4361-4364.
44. Y. H. Ng, S. Ikeda, T. Harada, S. Higashida, T. Sakata, H. Mori and M. Matsumura, *Adv. Mater.*, 2007, **19**, 597-601.
45. X. W. Lou and L. A. Archer, *Adv. Mater.*, 2008, **20**, 1853-1858.
46. K. Kamata, Y. Lu and Y. N. Xia, *J. Am. Chem. Soc.*, 2003, **125**, 2384-2385.
47. Z. Kai, X. H. Zhang, H. T. Chen, C. Xin, L. L. Zheng, J. H. Zhang and Y. Bai, *Langmuir*, 2004, **20**, 11312-11314.
48. P. Valle-Vigón, M. Sevilla and A. B. Fuertes, *Mater. Lett.*, 2010, **64**, 1587-1590.
49. G. Li, Q. Shi, S. J. Yuan, K. G. Neoh, E. T. Kang and X. Yang, *Chem. Mater.*, 2010, **22**, 1309-1317.
50. B. Guan, Y. Cui, Z. Ren, Z.-A. Qiao, L. Wang, Y. Liu and Q. Huo, *Nanoscale*, 2012, **4**, 6588-6596.
51. S. Wu, J. Dzubiel, J. Kaiser, M. Drechsler, X. Guo, M. Ballauff and Y. Lu, *Angew. Chem., Inter. Ed.*, 2012, **51**, 2229-2233.
52. D. Liu, J. Wang, Y. Zhang, J. Liu, H. Li, L. Zhou, S. Wu and X. Gao, *J. Mater. Sci.*, 2018, **53**, 8086-8097.
53. Z. Zhang, C. Shao, P. Zou, P. Zhang, M. Zhang, J. Mu, Z. Guo, X. Li, C. Wang and Y. Liu, *Chem. Commun.*, 2011, **47**, 3906-3908.
54. H. Zou, R. Wang, X. Li, X. Wang, S. Zeng, S. Ding, L. Li, Z. Zhang and S. Qiu, *J. Mater. Chem. A*, 2014, **2**, 12403-12412.
55. C. Li, P. Wang, Y. Tian, X. Xu, H. Hou, M. Wang, G. Qi and Y. Jin, *Acs Catal.*, 2017, **7**, 5391-5398.
56. Y. Deng, Y. Cai, Z. Sun, J. Liu, C. Liu, J. Wei, W. Li, C. Liu, Y. Wang and D. Zhao, *J. Am. Chem. Soc.*, 2010, **132**, 8466-8473.
57. J. Lee, C. P. Ji and H. Song, *Adv. Mater.*, 2008, **20**, 1523-1528.
58. F. H. Lin and R. A. Doong, *Appl. Catal. A Gen.*, 2014, **486**, 32-41.
59. Z. H. Ren, H. T. Li, Q. Gao, H. Wang, B. Han, K. S. Xia and C. G. Zhou, *Mater. Design*, 2017, **121**, 167-175.
60. Y. Yang, J. Liu, X. Li, X. Liu and Q. Yang, *Chem. Mater.*, 2011, **23**, 3676-3684.

TOC

